Science Translational Medicine AAAS

Silencing *HoxA1* by Intraductal Injection of siRNA Lipidoid Nanoparticles Prevents Mammary Tumor Progression in Mice

Amy Brock *et al.*

Sci Transl Med **6**, 217ra2 (2014);
DOI: 10.1126/scitranslmed.3007048

Editor's Summary

Silencing Breast Cancer with Nanoparticle siRNA

Cancer drives researchers crazy. But what drives cancer? In a new study by Brock and colleagues, the researchers modeled the gene network of mice and found *HoxA1* to be a putative driver of early breast cancer progression. Silencing this gene using nanoparticle-packaged small interfering RNA (siRNA) led to tumor reduction in mice.

Ductal carcinoma in situ (DCIS) is a noninvasive lesion of the breast that progresses to invasive breast cancer in an estimated 14 to 53% of cases. However, current prognostic methods are unable to predict whether DCIS will indeed become invasive. Brock *et al.* used a computational gene network inference approach to look at early gene expression changes in mammary tumor progression, and identified *HoxA1* as a likely candidate. The authors then confirmed that *HoxA1* was overexpressed in human breast lesions by looking at patient gene expression data. To verify the role of this candidate gene in cancer progression, *HoxA1* siRNA was formulated into lipidoid nanoparticles and administered to transgenic mice that develop tumors much like people do. The *HoxA1*-silencing nanoparticles were delivered locally (through the nipple), to avoid any systemic immune response, and led to a decrease in tumor formation, as compared to mice that received control siRNA. Notably, the *HoxA1* siRNA prevented the loss of hormone (estrogen and progesterone) receptors in the treated mammary glands —a loss that is one hallmark of breast cancer progression.

This study demonstrates how computational methods can generate viable oncogene candidates for RNA interference (RNAi) therapy. Brock *et al.* discovered and preliminarily validated *HoxA1* as a driver of breast cancer progression in mice, but additional human cell and tissue testing will be needed to verify the role of this gene in human DCIS and mammary tumorigenesis.

Science Translational Medicine (print ISSN 1946-6234; online ISSN 1946-6242) is published weekly, except the last week in December, by the American Association for the Advancement of Science, 1200 New York Avenue NW, Washington, DC 20005.

CANCER

Silencing *HoxA1* by Intraductal Injection of siRNA Lipidoid Nanoparticles Prevents Mammary Tumor Progression in Mice

Amy Brock,[1]*† Silva Krause,[2]* Hu Li,[1]*‡ Marek Kowalski,[1] Michael S. Goldberg,[3] James J. Collins,[1,4] Donald E. Ingber[1,2]§

With advances in screening, the incidence of detection of premalignant breast lesions has increased in recent decades; however, treatment options remain limited to surveillance or surgical removal by lumpectomy or mastectomy. We hypothesized that disease progression could be blocked by RNA interference (RNAi) therapy and set out to develop a targeted therapeutic delivery strategy. Using computational gene network modeling, we identified *HoxA1* as a putative driver of early mammary cancer progression in transgenic C3(1)-SV40TAg mice. Silencing this gene in cultured mouse or human mammary tumor spheroids resulted in increased acinar lumen formation, reduced tumor cell proliferation, and restoration of normal epithelial polarization. When the *HoxA1* gene was silenced in vivo via intraductal delivery of nanoparticle-formulated small interfering RNA (siRNA) through the nipple of transgenic mice with early-stage disease, mammary epithelial cell proliferation rates were suppressed, loss of estrogen and progesterone receptor expression was prevented, and tumor incidence was reduced by 75%. This approach that leverages new advances in systems biology and nanotechnology offers a novel noninvasive strategy to block breast cancer progression through targeted silencing of critical genes directly within the mammary epithelium.

INTRODUCTION

The most common noninvasive lesion of the breast is ductal carcinoma in situ (DCIS), in which abnormal ductal epithelial cells proliferate inside the mammary duct but do not penetrate through the basement membrane to invade adjacent tissue. In the United States, about 25% of newly diagnosed breast lesions are classified as DCIS, and more than 1 million women will be living with DCIS in the United States alone by 2020 (*1*, *2*). Atypical ductal hyperplasia represents about 10% of breast lesions detected by mammograms. These are marked by the presence of abnormal epithelial cells and elevated cell numbers compared with normal mammary ducts (*3*). All classes of early lesions are highly heterogeneous, and, although only a fraction will progress to invasive breast tumors (estimates range from 14 to 53% for DCIS) (*4*–*6*), there are currently no biomarkers to aid in identifying which tumors will become invasive. Surveillance (so-called watch and wait) may be recommended for earlier stages of hyperplasia with or without atypia.

Treatment of premalignant disease is typically aggressive for DCIS lesions, and options include mastectomy, lumpectomy, and radiation. All of these have serious systemic side effects and impact quality of life. Some patients with hormone receptor–positive DCIS will also receive 5 years of endocrine therapy, which has been shown to reduce recurrence, although no survival benefit has been demonstrated. The side effects of endocrine therapy may be life-threatening and include stroke, blood clots, bone loss, and elevated risks of uterine and endometrial cancers (*7*). For these reasons, a recent survey of breast cancer professionals identified the need for minimally invasive therapies that can be selectively targeted to the ductal epithelium to prevent progression of premalignant breast lesions without producing systemic toxicity as one of the highest priorities of translational breast cancer research (*8*).

Small interfering RNA (siRNA) has been used as a therapeutic agent in the treatment of a variety of tumor types in rodent models, including human mammary tumor xenografts in mice (*9*–*11*), and it is well tolerated with few adverse side effects. Therapeutic RNA interference (RNAi) is also currently being tested in human clinical trials in patients with liver cancer, metastatic liver disease, pancreatic ductal adenocarcinoma, advanced colon cancer, and familial adenomatous polyposis (FAP), which leads to colon tumorigenesis (*12*). RNAi-based approaches offer the possibility for a more personalized therapy in that the same technology and approach can be adapted to a variety of tumor-specific gene targets. In addition, RNAi is useful for silencing undruggable targets that are not amenable to traditional small molecule– or antibody-based inhibition (*13*–*15*).

Nevertheless, development of RNAi-based cancer therapeutics has been hampered by two major obstacles: (i) identification of appropriate target genes that are causally involved in cancer development, and (ii) selection of an effective delivery method with minimal systemic side effects. Here, we addressed the first challenge through gene network inference—a computational biology approach that evaluates gene expression changes in the context of the entire gene regulatory network (GRN). Through this analysis, we identified the *HoxA1* gene as a critical mediator of mammary tumor progression in humans. To validate the importance of this gene for breast cancer progression and to address the second challenge, we delivered *HoxA1* siRNA into mammary epithelial cells in vivo using lipidoid nanoparticles, which have been shown to facilitate interaction with the cell membrane and endosomal escape in other tissues, including an ovarian tumor model in mice (*16*). In contrast to earlier studies in which lipidoid-formulated siRNA was injected intratumorally, we delivered the nanoparticles to premalignant lesions within the lining

[1]Wyss Institute for Biologically Inspired Engineering, Harvard University, Boston, MA 02115, USA. [2]Vascular Biology Program, Boston Children's Hospital and Department of Pathology, Harvard Medical School, Boston, MA 02115, USA. [3]Dana-Farber Cancer Research Institute, Harvard Medical School, Boston, MA 02115, USA. [4]Howard Hughes Medical Institute, Boston University, Boston, MA 02115, USA.
*These authors contributed equally to this work.
†Present address: Department of Biomedical Engineering and Institute for Cellular and Molecular Biology, The University of Texas at Austin, Austin, TX 78712, USA.
‡Present address: Center for Individualized Medicine, Department of Molecular Pharmacology and Experimental Therapeutics, Mayo Clinic College of Medicine, Rochester, MN 55905, USA.
§Corresponding author. E-mail: don.ingber@wyss.harvard.edu

epithelium of intact mammary glands of virgin transgenic mice by direct injection through the nipple. Local delivery is noninvasive and avoids the uptake and accumulation of nanoparticles in the liver—an issue that has proven challenging in systemic administration (*17*).

HoxA1 silencing was tested in human mammary spheroids, as well as in a transgenic mouse model of mammary tumorigenesis. The FVB C3(1)-SV40TAg transgenic mouse was chosen as a relevant model of human breast cancer because (i) tumors form spontaneously in the correct tissue microenvironment; (ii) tumor onset and formation are slow, occurring over a period of 4 to 5 months; (iii) lesions robustly progress through all of the typical stages of breast tumorigenesis seen in humans, including hyperplasia DCIS and locally invasive carcinomas that can metastasize to the lung and liver; (iv) the immune system remains intact; and (v) tumor onset does not require exogenous hormone intervention or pregnancy is required in other transgenic breast cancer models (*18*, *19*).

We found that silencing *HoxA1* within the mammary ducts in vivo by delivering nanoparticle-formulated siRNA prevented loss of hormone receptor expression, suppressed cell proliferation, and reduced mammary tumor incidence in mice. This strategy of localized gene silencing may be translatable to human tumors for prevention of mammary tumor progression.

RESULTS

Putative target identification by computational gene network inference

To identify candidate gene targets with a high likelihood of driving tumor progression in the transgenic mouse FVB C3(1)-SV40TAg model, we constructed models of GRN connectivity with the mode-of-action by network identification (MNI) tool (*20*, *21*). The MNI tool was first trained on 3000 gene microarray data sets from various mouse tissues and organs under diverse conditions to develop a basal GRN connectivity model—a directed graph that relates the concentration of each gene transcript to that of every other transcript across the genome (Fig. 1, training phase, and fig. S1). Genes were deemed connected in this network if the activity of one gene influenced the transcriptional state of the other, regardless of whether the effect occurred at transcriptional or posttranscriptional levels and independently of the type or directionality of the interaction. Hierarchical clustering (by Euclidean distance with complete linkage performed with the *z* score–normalized expression value) revealed that samples clustered on the basis of disease progression (fig. S1A). Expression profiles of transgenic glands from early stages of cancer progression (<16 weeks) were most similar, whereas the profile of the 20-week glands that contained fulminant cancers was clearly distinct (Pearson's correlation coefficient >0.99 at 20 weeks versus ~0.92 at earlier times) (fig. S1, B and C).

The trained GRN model was then tested with transgenic and wild-type mammary gland transcriptome data to identify the earliest changes that rewire the GRN during tumorigenesis. In female transgenic C3(1)-SV40TAg mice, breast tumor formation progresses in a highly reproducible manner, with hyperplasia first appearing at ~12 weeks of age, DCIS-like lesions at ~16 weeks, and invasive carcinomas at 20 weeks (Fig. 2A) (*19*). To focus on early events in tumorigenesis, we obtained whole-genome transcriptome profiles for mammary glands isolated from 8-week-old transgenic mice when the transgene is highly expressed, but the glands remain histologically normal. Candidate transcription factors were ranked by two-tailed *P* value, and the *HoxA1* gene emerged as the most significant potential key mediator of early cancer progression ($P = 0.0005$) (Fig. 1, testing phase). We focused on *HoxA1* because past work in human tissues also suggested that it might play an important role in breast cancer development (*22*–*24*).

Validation of targets in three-dimensional mouse mammary epithelial cell spheroids

To assess the functional relevance of *HoxA1* to breast cancer biology, we then explored whether down-regulating its expression would alter the growth or differentiation of cultured mammary epithelial tumor cells that were originally isolated from primary (M6) or metastatic (M6C)

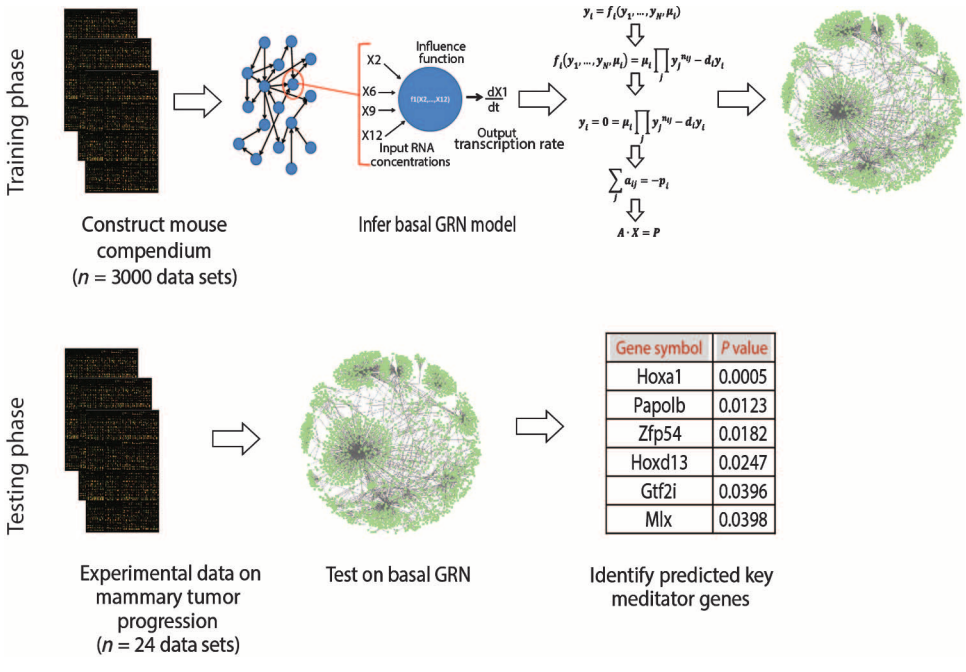

Fig. 1. Gene network inference pipeline. In the first phase (training), the MNI algorithm was trained on a compendium of 3000 mouse microarray data sets to construct a basal network connectivity model. Genome-wide expression data from wild-type (WT) and 8-week-old transgenic mammary glands were then interrogated in a testing phase using the GRN model to pinpoint alterations in gene behavior that were unique to particular stages of tumorigenesis. The significance of the predicted key mediator genes of the disease stage of interest is quantified with a *z* score. Two-tailed *P* values were calculated on the basis of the *z* score value. Genes are ranked according to the *P* value, and top-ranked genes were selected as probable key mediators of the disease state.

tumors in the same transgenic C3(1)-SV40Tag mice. *HoxA1* was silenced with siRNA in M6 and M6C cells or in normal mouse Eph4 mammary epithelial cells, which were cultured within extracellular matrix (ECM) gels composed of Matrigel and type I collagen. More than 75% of the normal Eph4 mammary cells formed well-differentiated, hollow acinar spheroids lined by a polarized epithelium with a central lumen (Fig. 2B).

These normal mammary cells were also highly polarized as indicated by the accumulation of a circumferential basement membrane containing a linear distribution of laminin-5 along their basal membranes, and a preferentially apical distribution of GM130 after 2 weeks of culture, which mimics normal polarized mammary epithelial architecture in vivo (Fig. 2, A and B). In contrast, M6 and M6C tumor cells failed to form hollow lumens and instead grew as disorganized spheroids filled with cells in vitro (Fig. 2, B and C), much as they do when they form solid tumors during later stages of cancer progression in vivo (Fig. 2A). As expected from their in vivo behavior, M6 and M6C cells also did not form a polarized epithelium or accumulate a linear basement membrane along their periphery (Fig. 2B).

Gene silencing using *HoxA1* siRNA (siHoxA1) induced both M6 and M6C cancer cells to reorganize into hollow acinar structures lined by a polarized epithelium, with restoration of both apical GM130 staining and a continuous, laminin-5–containing basement membrane at their basal cell surface (Fig. 2, B and C). Thus, silencing of a single gene identified by the MNI algorithm—*HoxA1*—resulted in breast cancer differentiation including reconstitution of the normal tissue architecture of wild-type mammary gland that is gradually lost in transgenic glands during disease progression (Fig. 2B). Spheroid differentiation induced by gene silencing was also accompanied by a significant reduction in the percentage of proliferating tumor cells in vitro (Fig. 2D), whereas the overall cell number per spheroid remained the same. This is consistent with the finding that a concomitant increase in tumor cell apoptosis was observed within the newly formed acinar lumens (Fig. 2E). Treatment of M6 and M6C cells with siHoxA1 reduced DNA synthesis by

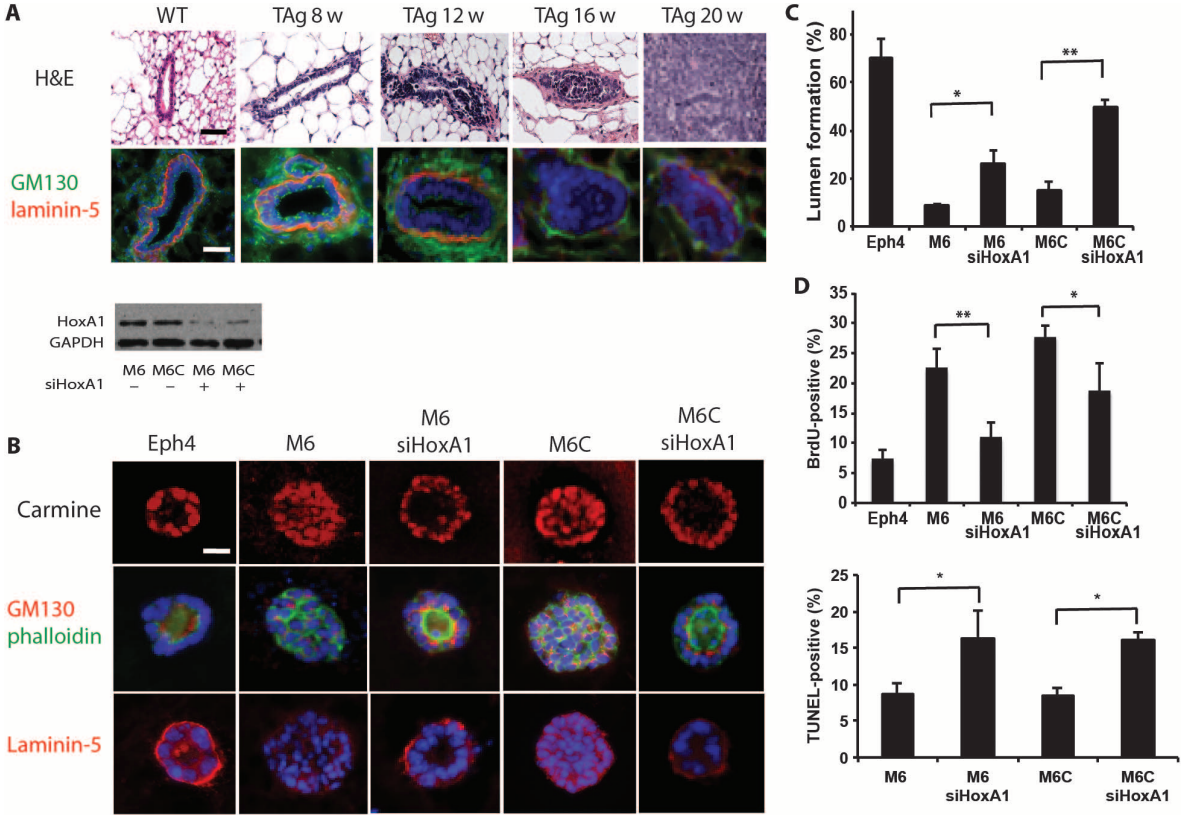

Fig. 2. In vitro silencing of *HoxA1* normalizes mouse mammary tumor cell spheroid cultures, restoring polarity and reducing proliferative index. (**A**) Disease progression in the C3(1)-SV40TAg glands is marked by atypia and hyperplasia, ductal filling, and tumor invasion [hematoxylin and eosin (H&E) images] with a progressive loss of GM130 and laminin polarity by 12 weeks and basement membrane thinning by 16 weeks (immunocytochemistry images). Scale bar, 100 μm. (**B**) Confocal images through the center of carmine-labeled normal mouse mammary (Eph4) and mouse mammary tumor (M6 and M6C) spheroid cultures reveal filled lumens in tumor cell cultures and a hollow organized lumen morphology when *HoxA1* is silenced. Cell polarity was visualized by immunocytochemistry of sectioned spheroids with staining of an apical Golgi marker GM130 and the basal basement membrane protein laminin. Nuclei were stained with DAPI (4′,6-diamidino-2-phenylindole) (blue), and F-actin was labeled with phalloidin (green). Scale bar, 20 μm. Images are representative of three studies (150 to 300 spheroids imaged per sample). Down-regulation of HoxA1 protein expression was confirmed by immunoblotting in lysates prepared from M6 and M6C cells ($n = 3$). (**C** and **D**) Effects of silencing *HoxA1* on hollow lumen formation (C) and cell proliferation (D) in collagen-Matrigel spheroid cultures of mouse M6 and M6C tumor cells. Eph4 mouse mammary cells served as normal controls. Data are means ± SD ($n = 3$, 150 to 300 spheroids imaged per sample). $^*P < 0.05$, $^{**}P < 0.01$, Fisher's exact *t* test. (**E**) Apoptosis after treatment of M6 and M6C cells with *HoxA1* siRNA ($n = 3$, 150 to 300 spheroids imaged per sample). $^*P < 0.05$, Fisher's exact *t* test.

more than 50 and 32%, respectively, and apoptosis increased by about twofold [~16.5% TUNEL (terminal deoxynucleotidyl transferase–mediated deoxyuridine triphosphate nick end labeling)–positive cells in siHoxA1-treated cells versus 8.5% in control M6 and M6C cells].

Silencing *HoxA1* in human breast cancer

To examine the relevance of *HoxA1* for human breast cancer, we performed differential expression analysis using the Oncomine compendium of cancer transcriptome profiles obtained from patient tumor samples. Human patient data from 10 previously published gene expression analyses, each consisting of 22 to 150 samples representing healthy breast tissue and tumors (*25*–*30*), revealed that *HoxA1* was overexpressed by greater than twofold in human breast lesions (Fig. 3A), which supports the relevance of the present results for human disease. To more directly explore this possibility, we then tested whether silencing of its expression using siRNA would alter the proliferation or differentiation of human MDA-MB-468 and HCC1937 breast tumor cells when grown within the same ECM gels used for the mouse mammary tumor three-dimensional (3D) cultures.

Upon silencing *HoxA1*, we observed a major increase in the ability of both human breast tumor cell lines (MDA-MB-468 cells and HCC1937) to organize into spheroids containing hollow central lumens under these 3D gel culture conditions (Fig. 3B). The siHoxA1-treated cells exhibited about six- and twofold increases relative to spheroids treated with nontargeting control siRNA, respectively (Fig. 3C). Between 30 and 38% of spheroids formed hollow lumens in the siHoxA1-treated human breast cancer cell cultures, compared with ~50% of spheroids formed by normal human mammary epithelial MCF10A cells (Fig. 3, B and C). Analysis of DNA synthesis under these culture conditions revealed that the growth of the MDA-MB-468 cells and HCC1937 cells were reduced by 60 and 50%, respectively, upon silencing *HoxA1* (Fig. 3D). Similar proliferation results were also observed in human breast cancer cells cultured in 2D on conventional cell culture plastic (fig. S2).

In vivo *HoxA1* silencing in mammary gland by intraductal delivery of siRNA lipidoid nanoparticles

To explore whether *HoxA1* represents a feasible target for treating the early stages of breast cancer progression, we formulated *HoxA1* and control, nontargeting siRNAs (siNTs) with lipidoid nanoparticles (*16*, *31*). These particles were delivered intraductally via injection through the nipple to reach the transformed mammary epithelial cells that give rise to early localized lesions within the lining ductal epithelium. Injection of a fluorescently tagged control siRNA formulated with lipidoid confirmed that a volume of 20 μl of siRNA nanoparticle solution filled the intact mammary tree and that the nipple and mammary ducts remained intact throughout the treatment (Fig. 4A and fig. S3A). In high-magnification confocal images of injected mammary ducts, fluorescent nanoparticles were observed within mammary epithelial cells at 48 hours and 1 week after injection, and they were not observed in the stromal cells that surround the epithelium (Fig. 4B). No fluorescent particles were observed in the liver, spleen, kidney, heart, lung, or peripheral blood at 48 hours, 72 hours, or 1 week after injection.

To determine the potential value of this approach in vivo, we injected virgin adult female transgenic mice with siHoxA1 or nontargeting control siRNA biweekly for 9 weeks beginning at 12 weeks of age. Gene silencing was confirmed by immunoblotting of protein isolated from mammary glands after the ninth week of treatment (fig. S3B). Although 100% of control transgenic mice or mice treated with siNT developed macroscopic tumors by 21 weeks of age, only 25% of mice treated with intraductal injection of siHoxA1 exhibited tumor formation by that time point (Fig. 4C). Tumor onset in the siHoxA1-

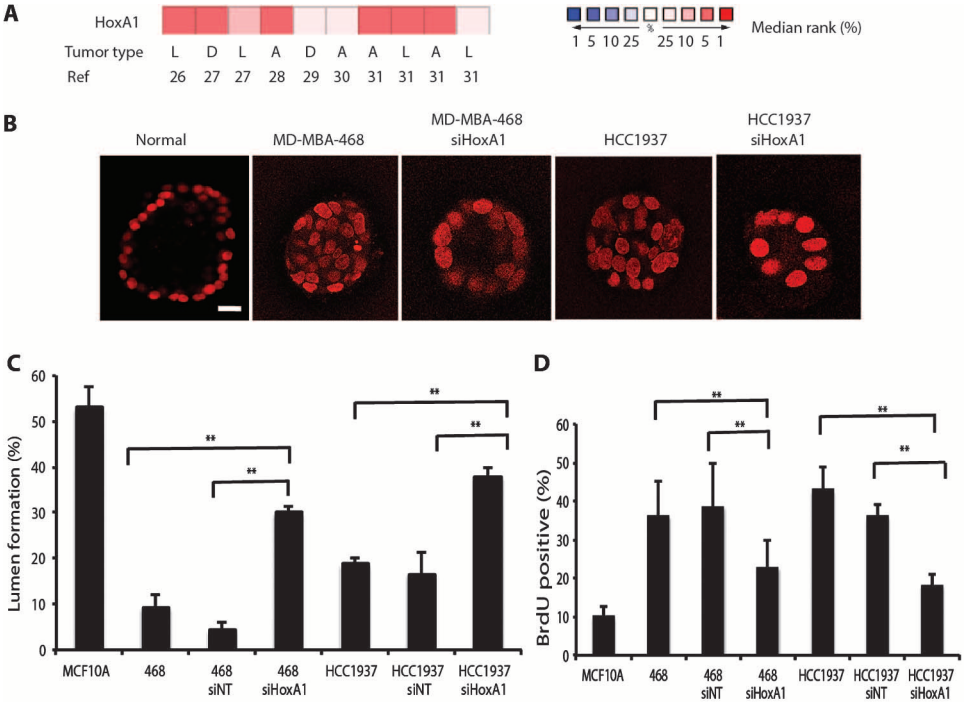

Fig. 3. Silencing *HoxA1* reduces human breast cancer cell growth and restores lumen organization in human tumor cell spheroid cultures. (**A**) The Oncomine compendium of cancer transcriptome profiles was used for analysis and visualization of *HoxA1* expression data in human breast tumors and normal breast tissue. Differential expression analysis identified 10 patient data sets in which *HoxA1* was overexpressed in human breast lesions by more than twofold (*25*–*30*). The type of tumor represented in the data sets is categorized as follows: A, all breast carcinomas; D, ductal breast carcinomas; and L, lobular breast carcinomas. The rank order of *HoxA1* in each analysis is displayed on a scale of red (increased rank %) to blue (decreased rank %). (**B**) Confocal images through the center of carmine-labeled spheroid cultures of normal human breast epithelial cells (MCF10A) and human breast cancer MDA-MB-468 and HCC1937 cell lines. Breast cancer cells were also treated with siHoxA1. Scale bar, 20 μm. (**C** and **D**) Hollow lumen formation (C) and proliferation (D) of cancer cells in collagen-Matrigel spheroid cultures. Quantitation of lumen formation in nontumorigenic human MCF10A breast epithelial cells and cells treated with scrambled siRNA controls is shown for comparison. Data are means ± SD (n = 3, 150 to 300 cells per sample). **P < 0.01, Fisher's exact t test.

treated mice was delayed by about 3 weeks, as detected by weekly ultrasound monitoring (Fig. 4D). Immunohistological characterization of the siHoxA1-treated mammary glands revealed the presence of hyperplasia and ductal filling at 21 weeks (Fig. 4E); however, these lesions did not progress to invasive macroscopic tumors in glands treated with siHoxA1. Cell proliferation was also lower in glands injected with siHoxA1 compared with controls, as measured by proliferating cell nuclear antigen (PCNA) (Fig. 3, E and F), but there was no significant change in the levels of apoptosis ($P > 0.05$, Fisher's t test) (Fig. 4G), suggesting that *HoxA1* inhibition acted by increasing (or preventing loss of) cell differentiation, rather than by inducing mammary tumor apoptosis.

Mammary tumorigenesis in C3(1)-SV40TAg transgenic glands is also marked by progressive loss of expression of hormone receptors, most notably the estrogen receptor (ER) and the progesterone receptor (PR). This is a common characteristic of the most highly aggressive forms of breast cancer in humans as well. Although only 4.7 and 5.9% of cells were ER^+ in untreated and siNT-treated glands, respectively, at 21 weeks of age, siHoxA1-treated glands continued to express ER at high levels, with 18.4% of cells staining positive for ER (Fig. 4, E and H). A similar response was observed for PR, with 15.7% of PR^+ cells in siHoxA1-treated glands versus only 5.9 and 7.9% in untreated and siNT-treated glands, respectively (Fig. 4, E and I).

FVB C3(1)-SV40TAg mice receiving intraductal injections of siRNA lipidoid nanoparticles were also monitored closely for signs of local tissue damage, toxicity, or systemic side effects. No weight loss was observed in the siHoxA1- or siNT-treated populations (fig. S4A). We also failed to detect an inflammatory response to siHoxA1- or siNT-containing nanoparticles by measuring spleen size or by quantifying interleukin-6 and interferon-γ cytokine levels (fig. S4, B to D). Cytokine levels remained low (less than 25 pg/ml) in all siHoxA1- or siNT-treated animals (fig. S4, C and D).

Down-regulation of mitogen-activated protein kinase signaling by *HoxA1* silencing

Activation of the mitogen-activated protein kinase (MAPK) pathway regulating cell proliferation and survival is a frequent event in tumori-

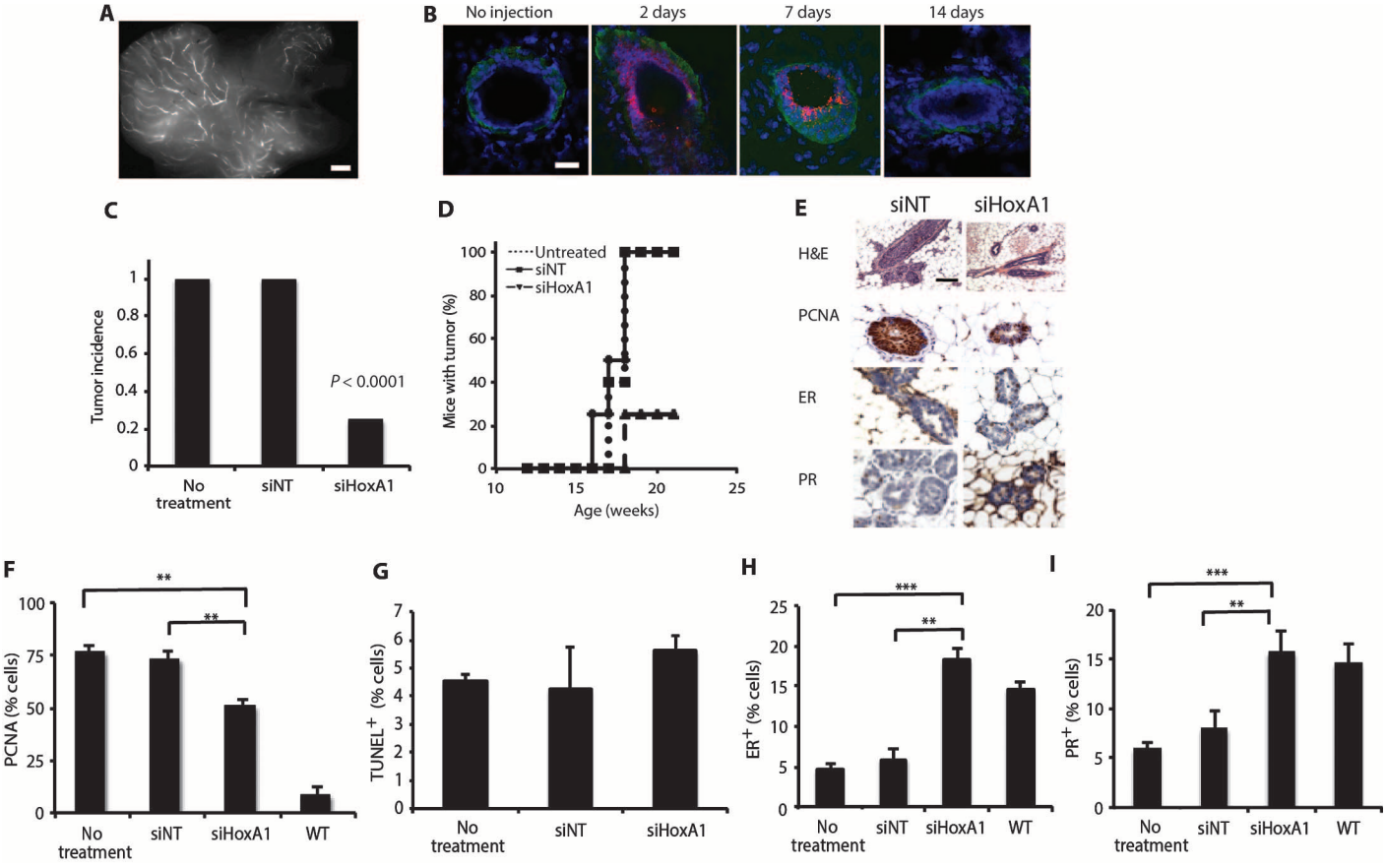

Fig. 4. Silencing *HoxA1* in the mammary epithelium reduces tumor incidence, reduces proliferative index, and prevents the loss of hormone receptor expression. (**A**) Virgin C3(1)-SV40TAg mammary glands injected in parallel with 20 μl of a fluorescent control siRNA nanoparticle to visualize the efficiency of its delivery throughout the ductal tree. The entire injected gland was removed and whole-mounted for fluorescence imaging. Scale bar, 1 mm. (**B**) Confocal images of mammary tissue sections show distribution of fluorescent control siRNA (red) in the duct at 2, 7, and 14 days after injection. Tissues were counterstained with laminin (green) and DAPI (blue). Scale bar, 100 μm. (**C**) Tumor incidence measured at 21 weeks in control C3(1)-SV40TAg mice versus mice injected with siHoxA1 biweekly for 9 weeks ($n = 10$ siNT, $n = 8$ siHoxA1, $n = 5$ untreated). P value versus both no treatment and siNT controls determined by log-rank test. (**D**) Timing of onset of tumor formation in untreated, siNT control, and siHoxA1-treated mice. (**E**) H&E and immunohistochemistry for PR, ER, and PCNA in mouse mammary glands. Scale bar, 100 μm. (**F** to **I**) Percentage of $PCNA^+$ (F), apoptotic (G), ER^+ (H), and PR^+ (I) cells after 9 weeks of treatment. Data are means ± SEM ($n = 5$ animals, 400 to 550 cells scored per animal). $^{**}P < 0.01$, $^{***}P < 0.001$, Pearson's χ^2 test.

genesis, and modulation of the p44/42 MAPK signaling pathway has previously been shown to contribute to *HoxA1*-mediated oncogenic transformation and anchorage-independent growth in cultured human mammary tumor cells (*32*). We therefore investigated the response of p44/42 signaling to local *HoxA1* silencing in mouse mammary glands in vivo. Gene expression analysis of transgenic mammary glands revealed alterations in expression of 13 core genes involved in the p44/42 MAPK signaling pathway as the disease progressed from early to late stages (Fig. 5A). Intraductal delivery of siHoxA1 reduced expression of Kras, extracellular signal–regulated kinase 1/2 (ERK1/2), Src, Grb2, Ier3, and PCNA in the transgenic mammary gland (Fig. 5B).

DISCUSSION

These data show that a GRN computational approach designed to define GRN connectivity can be used to successfully identify genes that are physiologically relevant to human breast tumor progression and that can serve as potential therapeutic targets with RNAi. Intraductal delivery of siRNA encapsulated in lipidoid nanoparticles enabled localization to the relevant cells lining the mammary ducts that give rise to the majority of invasive breast tumors. With increasing availability of genome-wide characterization of clinical samples, we envision the broad application of this approach to multiple types of premalignant lesions, in the breast and other organs. This approach can be generalized to target any candidate gene, allowing the treatment of breast lesions in a tumor- and patient-specific manner. For example, it may be possible to personalize siRNA treatments for patients with known gene mutations. Here, we determined that *HoxA1* was a critical transcriptional regulator during early stages of mammary tumorigenesis and, accordingly, tailored RNAi therapy to this target.

Hox genes act as master regulators of development in the embryo and are expressed in a tightly regulated spatiotemporal fashion. In humans, *HoxA1* plays a critical role in early embryonic development and is critical in hindbrain segmentation, skull morphogenesis, and inner ear organogenesis (*33*). Alterations in Hox genes also have been associated with a variety of human cancers, including breast (*22*, *34*), skin (*35*), lung (*36*), prostate (*37*), and hematopoietic tumors (*38*). *HoxA1* is not expressed in adult human mammary gland, but several previous studies have revealed up-regulation in mammary carcinomas (*22*, *23*, *39*, *40*). Although additional studies will be required to clarify the mechanism by which *HoxA1* contributes to breast tumor formation in humans, previous work has shown that overexpression of *HoxA1* in normal human mammary epithelial cells is sufficient to initiate oncogenic transformation (*24*). Furthermore, we demonstrate here that silencing *HoxA1* suppresses growth and induces differentiation of human breast cancer spheroids and that suppression of this gene in the early stages of the disease is associated with reduced MAPK signaling in mice, suggesting that it may also be a relevant target in human tumors that respond to MEK (MAPK kinase) inhibitors.

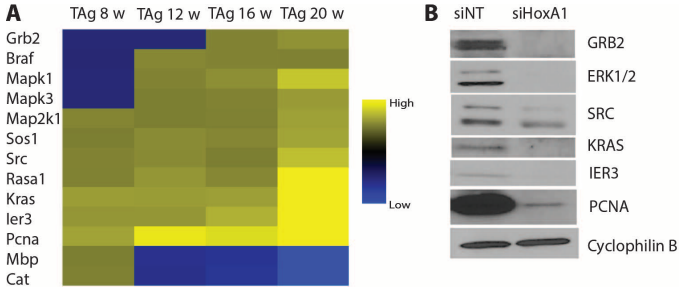

Fig. 5. siHoxA1 reduces mammary tumor cell proliferation in vivo through modulation of p44/42 MAPK signaling. (**A**) Microarray analysis of MAPK pathway signature genes in untreated transgenic C3(1)-SV40TAg mammary glands ($n = 3$) at progressive disease stages. (**B**) Effect of biweekly siHoxA1 injections on protein expression of MAPK components—ERK1/2, SRC, IER3, KRAS, PCNA, and GRB2—in mammary glands of 21-week-old transgenic animals ($n = 3$) compared with injection of siNT ($n = 3$).

The promise of less invasive, intraductal alternatives for human breast cancer patients has been widely discussed in recent years, and small pilot studies have demonstrated the feasibility of cannulating diseased ducts in humans (*41*) for the delivery of chemotherapeutic agents to specific ducts (*42*). Conventional chemotherapeutic agents, such as 5-fluorouracil (5-FU), carboplatin, and pegylated liposomal doxorubicin, have also been shown to be effective when injected intraductally in rodent models of chemically induced carcinogenesis (*43*, *44*). However, long-term follow-up (>30 weeks) revealed that intraductal delivery of this form of doxorubicin also induced formation of malignant mammary tumors in normal FVB/N mice (*45*). Our results show that RNAi-based therapies can be similarly delivered intraductally in a transgenic mouse mammary cancer model, which both provides a more relevant animal model for breast cancer progression than fat pad injections and opens up the possibility for development of this class of noncytotoxic siRNA-based agents as a new minimally invasive, localized treatment option.

All untreated SV40TAg animals developed tumors by 21 weeks of age, and hence, they needed to be sacrificed at this time according to humane animal care procedures. Therefore, the 21-week end point was chosen to permit comparison of the tumor burden in untreated and siRNA *HoxA1*–treated groups. So, although this study demonstrated safety and the ability to reduce the rate of tumor formation in treated mice throughout the 21-week study period, we cannot comment on the long-term effects of RNAi therapy. In any case, additional studies will be needed to characterize the pharmacokinetics, long-term safety, and long-term dosing and efficacy of intraductally administered RNAi therapeutics before this therapeutic strategy is explored for clinical use. Unlike mice, human breasts contain multiple ductal systems with separate openings on the nipple. Thus, a large animal model with similar mammary gland anatomy, such as rabbits, may provide additional insight.

Notably, the diameter and volume of the human breast ducts are larger than those of the mouse, but still lined by a single layer of epithelial cells; this may allow administration of higher doses or use of less frequent dosing. Studies on a larger animal could also be useful for assessing the clearance of siRNA nanoparticles and for determining whether biweekly dosing or a less frequent dosing regimen would be reasonable starting points for human studies. In the end, appropriate dosing in humans would have to be determined and optimized in phase 1 clinical trials. Furthermore, the Oncomine data on *HoxA1* in human tumors may not be sufficiently representative of human DCIS. To examine this disease stage in greater detail, clinical biopsy samples may need to be examined specifically from patients with DCIS but without invasive tumors.

The siRNA nanoparticles were delivered to animals before tumor formation. Thus, if this strategy is considered for future use in humans, the RNAi could be administered in a prophylactic capacity to high-risk patients, before the detection of DCIS or breast lesions (as demonstrated

here in mice). Alternatively, it could be administered with chemotherapy to women who have had tumors removed and who would normally receive chemotherapy (or radiation therapy) to prevent progression of remaining small undetected lesions. The feasibility, the absence of side effects over several months, and the overall prevention of tumor progression observed in this study support the further investigation of intraductal delivery of patient-specific siRNA therapy for breast cancer prevention and treatment.

MATERIALS AND METHODS

Study design

The overall objective of this study was to use gene network inference to predict target genes to block mammary tumor progression and to test these computational predictions in cell and animal models of disease. On the basis of modeling predictions, we hypothesized that silencing *HoxA1* within mammary epithelial cells in the transgenic duct would prevent mammary tumorigenesis. Data from previous studies with the FVB C3(1)-SV40TAg mouse model in our laboratory determined a low variability in tumor incidence. Statisticians at the Boston Children's Hospital were then consulted regarding the sample size and design of animal studies. Animals were assigned randomly to experimental groups by the veterinary technician. By 21 weeks of age, FVB C3(1)-SV40TAg animals have one or more mammary tumors, and these are typically greater than 10% of body weight. At this time point, animals must be sacrificed according to ethical animal care protocols. As predefined study component, we therefore chose 21 weeks as an end point to allow comparison of the tumor burden in treated animals to that in the control group (without siHoxA1 treatment). We also determined that premature death would result in exclusion from the study. One untreated control animal displayed symptoms of seizure [a condition known to affect the FVB C3(1)-SV40TAg strain] and was excluded from further study. The dosing regimen was determined by monitoring the localization of the nanoparticles within the mammary gland over time. Particles were completely cleared by 2 weeks after injection. Quantitation and scoring of immunohistochemistry of PR, ER, and PCNA were performed by blinded individuals, and tumor scoring was confirmed by a blinded pathologist in the Harvard Medical School Rodent Core. For immunohistochemistry, five sample images were analyzed for each tissue sample. All experiments were performed in triplicate.

Animals

For transcriptome analysis, whole mammary glands were harvested from wild-type FVB mice at 8 weeks of age and from transgenic FVB C3(1)-SV40TAg mice (The Jackson Laboratory) at 8, 12, 16, and 20 weeks of age ($n = 5$ per time point). All animal experimental protocols were approved by the Institutional Animal Care and Use Committee of Children's Hospital Boston.

Gene expression analysis

Tumor gene expression profiling was carried out with Affymetrix Mouse Genome (MG) 430 2.0 GeneChip arrays. In brief, total RNA was extracted from tissue with the RNeasy kit including deoxyribonuclease digestion (Qiagen). Biotin-labeled complementary DNA (cDNA) was obtained from 1 μg of total RNA with the GeneChip one-cycle labeling kit (Affymetrix). According to the manufacturer's instructions, 1.5 μg of cDNA was fragmented and hybridized to Affymetrix MG 430 2.0 GeneChip arrays. Arrays were processed by the Harvard Genotyping and Microarray Center (Boston, MA). DNA chips were washed, stained, and scanned with an Affymetrix Fluidics device and a GCS3000 scanner, and the images obtained were analyzed with the GeneChip Operating Software (GCOS). The experiment was performed in five replicates for wild-type mice at 8 weeks of age and for transgenic mice at 8, 12, 16, and 20 weeks of age. Data normalization was calculated with the robust multichip average (RMA) algorithm (*32*) implemented in Bioconductor (http://www.bioconductor.org). MG 430 2.0 mRNA data from each individual sample have been deposited with the National Center for Biotechnology Information (NCBI) Gene Expression Omnibus (GEO) (http://www.ncbi.nlm.nih.gov/geo/) under accession number GSE50813.

Compendium generation for MNI

About 11,000 mouse microarrays data were collected from the National Institutes of Health (NIH) GEO. All the arrays were processed on the basis of the Affymetrix MG 430 2.0 chip, which contains more than 45,000 probe sets representing more than 34,000 validated mouse genes. Sequences used in the design of the array were selected from GenBank, dbEST, and RefSeq. Eleven pairs of oligonucleotide probes measure the level of transcription of each sequence represented on the MG 430 2.0 GeneChip array. Data normalization on the total compendium was calculated with the RMA algorithm implemented in Bioconductor (http://www.bioconductor.org). K-means clustering method was applied on the total mouse compendium data, and about 3000 microarrays were selected as final training input data set for MNI.

MNI network inference

The MNI algorithm and underlying assumptions have been published previously (*33*) and are in the Supplementary Materials and Methods. Briefly, the algorithm consists of two phases. In the first phase (the training phase), a model of regulatory influences in the cell is learned from an $N \times M$ data matrix, X, consisting of measurements of steady-state expression ratios of N genes in M experiments. To estimate the network model A, the MNI algorithm uses a recursive strategy. The algorithm begins by using the data matrix, X, and a naïve model of the regulatory structure (that is, no genes regulate any other) to estimate P, an $N \times M$ matrix of external influences on the genes. The estimate of P is then used, with A, to determine A by principal components regression analysis. Estimates of A and P are then used to estimate one another recursively until the estimates converge. In the second phase of the algorithm, the A matrix, representing a model of regulatory influences in the cell, is used to estimate the "key mediator genes" of the disease stage of interest. The disease stage then becomes an $N \times 1$ vector, p, of gene-specific influences that result in the log-transformed expression ratios, x, measured for that disease state. The p vector is then calculated directly from the log-linear regulatory model as $P = Ax$. The significance of each element of the p vector is then calculated as a z score. Genes are ranked according to the z score of their corresponding element in the p vector, and top-ranked genes and pathways are selected as probable key mediators of the disease state.

Cell culture

M6 and M6C cell lines were a gift from C. Jorczyk (Boise State University), and Eph4 cells were a gift from K. Freeman (Boston Children's Hospital). M6, M6C, and Eph4 cells were maintained in high-glucose (4.5 g/ml) Dulbecco's modified Eagle's medium (DMEM) growth medium

supplemented with 5% fetal bovine serum (FBS) and 1% penicillin/streptomycin (P/S) (*46*). Human breast (MCF10A) and breast cancer (HCC1937 and MDA-MB-468) cell lines were purchased from the American Type Culture Collection. MCF10A cells were maintained in DMEM/F12 growth medium containing 5% equine serum, epidermal growth factor (EFG) (20 ng/ml), hydrocortisone (0.5 μg/ml), cholera toxin (0.1 μg/ml), insulin (10 μg/ml), and 1% P/S. HCC1937 cells were maintained in RPMI 1640 medium with 10% FBS and 1% P/S, whereas MDA-MB-468 cells were grown in Leibovitz's L-15 medium with 10% FBS and 1% P/S. All other cells were maintained at 37°C and 5% CO_2. MDA-MB-468 cells were grown at 37°C and atmospheric air (0% CO_2).

In vitro silencing

siRNA targeting *HoxA1* was purchased from Dharmacon and transfected into M6, M6C, MDA-MB-468, or HCC1937 cells with 25 nM DharmaFECT 1 reagent according to the manufacturer's protocols. Target sequences were as follows: siRNA HoxA1_1: 5′-CAACAAGUACCUUACACGA-3′; siRNA HoxA1_ 2: 5′-CCAUAGGAUUACAACUUUCT-3′. A nontargeting sequence (ON-TARGETplus D-001810-01) was transfected as a negative control. To confirm the effectiveness of the silencing reagent in 3D cell culture, ON-TARGET glyceraldehyde-3-phosphate dehydrogenase (GAPDH)–positive control siRNA was also transfected. Cells were maintained in 3D culture for 14 days and then collected for analysis by dissolution of the gel with collagenase. Immunoblotting confirmed effective silencing in cells with rabbit anti-HoxA1 (Abcam).

Spheroid culture in 3D gels

Mammary epithelial and tumor cells described above were trypsinized, centrifuged, and resuspended in a 1:1 solution of type I collagen (3 mg/ml) and Matrigel and added to the top section of a 12-mm Transwell plate with 0.4-μm polycarbonate membrane, such that the final cell number was 100,000 cells per well. Gels were allowed to harden at 37°C for 30 min before growth medium was added to the top and bottom sections of the Transwell plate. Gel cultures were maintained at 37°C, 5% CO_2 for 8 to 14 days. Gels were then fixed in 10% formalin overnight, and the Transwell membrane containing the gel was removed from the culture chamber before carmine staining or sectioning.

In vivo RNAi delivery

siRNA was formulated with lipid-like amino alcohols (lipidoids) as described previously (*47*). Particle sizes were measured by dynamic light scattering with a Malvern Zetasizer Nano ZS. siRNA (20 μg) was delivered intraductally to the thoracic gland of the mouse through the nipple with a 33-gauge needle while visualizing the nipple site under a stereoscope (*48*). Fluorescently tagged siRNA (DharmaFECT siGLO) and Evans blue vital dye were used to determine the volume needed to fill the mammary ductal tree completely without perforating the wall of the duct. After injection, glands were imaged weekly with a Vevo 2100 VisualSonics ultrasound machine to determine the onset, number, size, and location of tumors.

Protein isolation and immunoblotting

Tissues were washed once in 500 μl of ice-cold Bio-Rad Bio-Plex cell wash buffer, cut into 3 × 3 mm pieces, and homogenized in 500 μl of ice-cold Bio-Rad Bio-Plex cell lysis buffer with an IKA T10 basic ULTRA-TURRAX homogenizer (dispersing element S10N-5G) for 30 s at minimum speed and 15 s at maximum speed. Homogenates were frozen at −80°C to complete the lysis, thawed, and centrifuged at 4°C, 8000*g*, for 20 min, followed by isolation of the soluble layer. Protein concentrations were measured with Bio-Rad DC Protein Assay on NanoDrop 2000. The following primary antibodies were used for immunoblotting: 1:10,000 rabbit anti-PCNA (Novus Biologicals), 1:2000 rabbit anti-Src (Cell Signaling Technology), 1:500 goat anti-Grb2 (R&D Systems), 1:1000 rabbit anti-ERK1/2 (R&D Systems), 1:2000 rabbit anti-IER3 (Novus Biologicals), 1:5000 rabbit anti-KRAS (Novus Biologicals), and 1:1000 rabbit anti-HoxA1 (Abcam).

Immunohistochemistry

Parallel gel samples were processed for frozen and paraffin-embedded sections. After formalin fixation to obtain frozen sections, gels were washed with phosphate-buffered saline and placed in O.C.T. (Tissue-Tek) with 30% sucrose at 4°C overnight. Gels were then flash-frozen on liquid N_2, and 8- to 10-μm sections were prepared with a cryostat (Leica). Staining of gels was carried out with the following antibodies and concentrations: 1:100 mouse anti-GM130 (BD Biosciences), 1:100 rabbit anti–laminin-5 (Abcam), 1:200 rabbit anti-ZO1 (Invitrogen), and TUNEL stain (Roche kit). Paraffin-embedded gel sections were stained with 1:200 rat anti-BrdU (5-bromo-2′-deoxyuridine) (Abcam). Paraffin tissue sections were prepared by the Harvard Medical School histology core facility and stained with 1:100 anti-ER (Abcam), 1:400 anti-PR (Dako), 1:100 anti-PCNA (Dako), and TUNEL (Roche). Stained sections were imaged at 40× with a Zeiss Imager, and cells from at least five representative fields were quantified per animal.

Microscopic analysis and quantitation

Confocal images of 3D spheroids in collagen/Matrigel were obtained on a Leica white laser Leica SP5 X multispectral-multiphoton confocal system. Images were acquired throughout the intact gel with 2-μm resolution to verify formation of a hollow central lumen. Sections and 2D cultures were imaged on a Zeiss Axio Observer Z1 with a CoolSNAP camera. Brightfield imaging was carried out with a Zeiss Axio Observer with Nuance color camera and multispectral imaging system. inForm software package (CRi) was used to perform automated quantitation of proliferative and apoptotic indices. MetaMorph software was used to perform morphometric analysis of lumen formation. Spheroids from three independent experiments were quantified for each sample, and 180 to 200 cells were scored per condition for each assay.

Statistical analysis

All in vitro assays were performed in triplicate. Data are reported as means ± SD for $n = 3$ assays. In vivo quantitation was performed on samples from five animals to account for potential heterogeneity. Data are reported as means ± SEM for assays in which $n > 5$ samples were quantified. For noncontinuous variables, P values were determined by Pearson's χ^2 test for large sample sizes and by Fisher's exact t test for smaller sample sizes.

SUPPLEMENTARY MATERIALS

www.sciencetranslationalmedicine.org/cgi/content/full/6/217/217ra2/DC1

Materials and Methods

Fig. S1. Conventional bioinformatics analysis of mammary gland gene expression changes in C3(1)-SV40Tag–driven tumorigenesis.

Fig. S2. Silencing of *HoxA1* in human cell lines in vitro.

Fig. S3. In vivo delivery of siRNA to the mammary ductal tree.
Fig. S4. Monitoring systemic response to in vivo RNAi.

REFERENCES AND NOTES

1. J. F. Simpson, Update on atypical epithelial hyperplasia and ductal carcinoma in situ. *Pathology* **41**, 36–39 (2009).
2. C. J. Allegra, D. R. Aberle, P. Ganschow, S. M. Hahn, C. N. Lee, S. Millon-Underwood, M. C. Pike, S. D. Reed, A. F. Saftlas, S. A. Scarvalone, A. M. Schwartz, C. Slomski, G. Yothers, R. Zon, National Institutes of Health State-of-the-Science Conference statement: Diagnosis and management of ductal carcinoma in situ September 22–24, 2009. *J. Natl. Cancer Inst.* **102**, 161–169 (2010).
3. R. K. Jain, R. Mehta, R. Dimitrov, L. G. Larsson, P. M. Musto, K. B. Hodges, T. M. Ulbright, E. M. Hattab, N. Agaram, M. T. Idrees, S. Badve, Atypical ductal hyperplasia: Interobserver and intraobserver variability. *Mod. Pathol.* **24**, 917–923 (2011).
4. W. L. Betsill Jr., P. P. Rosen, P. H. Lieberman, G. F. Robbins, Intraductal carcinoma. Long-term follow-up after treatment by biopsy alone. *JAMA* **239**, 1863–1867 (1978).
5. V. Eusebi, E. Feudale, M. P. Foschini, A. Micheli, A. Conti, C. Riva, S. Di Palma, F. Rilke, Long-term follow-up of in situ carcinoma of the breast. *Semin. Diagn. Pathol.* **11**, 223–235 (1994).
6. M. E. Sanders, P. A. Schuyler, W. D. Dupont, D. L. Page, The natural history of low-grade ductal carcinoma in situ of the breast in women treated by biopsy only revealed over 30 years of long-term follow-up. *Cancer* **103**, 2481–2484 (2005).
7. B. Fisher, J. P. Costantino, D. L. Wickerham, C. K. Redmond, M. Kavanah, W. M. Cronin, V. Vogel, A. Robidoux, N. Dimitrov, J. Atkins, M. Daly, S. Wieand, E. Tan-Chiu, L. Ford, N. Wolmark, Tamoxifen for prevention of breast cancer: Report of the National Surgical Adjuvant Breast and Bowel Project P-1 Study. *J. Natl. Cancer Inst.* **90**, 1371–1388 (1998).
8. M. Dowsett, A. Goldhirsch, D. F. Hayes, H. J. Senn, W. Wood, G. Viale, International Web-based consultation on priorities for translational breast cancer research. *Breast Cancer Res.* **9**, R81 (2007).
9. I. Tekedereli, S. N. Alpay, U. Akar, E. Yuca, C. Ayugo-Rodriguez, H. D. Han, A. K. Sood, G. Lopez-Berestein, B. Ozpolat, Therapeutic silencing of Bcl-2 by systemically administered siRNA nanotherapeutics inhibits tumor growth by autophagy and apoptosis and enhances the efficacy of chemotherapy in orthotopic xenograft models of ER (–) and ER (+) breast cancer. *Mol. Ther. Nucleic Acids* **2**, e121 (2013).
10. S. Ohno, M. Takanashi, K. Sudo, S. Ueda, A. Ishikawa, N. Matsuyama, K. Fujita, T. Mizutani, T. Ohgi, T. Ochiya, N. Gotoh, M. Kuroda, Systemically injected exosomes targeted to EGFR deliver antitumor microRNA to breast cancer cells. *Mol. Ther.* **21**, 185–191 (2013).
11. H. M. Aliabadi, R. Maranchuk, C. Kucharski, P. Mahdipoor, J. Hugh, H. Uludağ, Effective response of doxorubicin-sensitive and -resistant breast cancer cells to combinational siRNA therapy. *J. Control. Release* **172**, 219–228 (2013).
12. J. C. Burnett, J. J. Rossi, K. Tiemann, Current progress of siRNA/shRNA therapeutics in clinical trials. *Biotechnol. J.* **6**, 1130–1146 (2011).
13. S. M. Elbashir, J. Harborth, W. Lendeckel, A. Yalcin, K. Weber, T. Tuschl, Duplexes of 21-nucleotide RNAs mediate RNA interference in cultured mammalian cells. *Nature* **411**, 494–498 (2001).
14. A. Fire, S. Xu, M. K. Montgomery, S. A. Kostas, S. E. Driver, C. C. Mello, Potent and specific genetic interference by double-stranded RNA in *Caenorhabditis elegans*. *Nature* **391**, 806–811 (1998).
15. K. A. Whitehead, R. Langer, D. G. Anderson, Knocking down barriers: Advances in siRNA delivery. *Nat. Rev. Drug Discov.* **8**, 129–138 (2009).
16. M. S. Goldberg, D. Xing, Y. Ren, S. Orsulic, S. N. Bhatia, P. A. Sharp, Nanoparticle-mediated delivery of siRNA targeting Parp1 extends survival of mice bearing tumors derived from Brca1-deficient ovarian cancer cells. *Proc. Natl. Acad. Sci. U.S.A.* **108**, 745–750 (2011).
17. Y. Huang, J. Hong, S. Zheng, Y. Ding, S. Guo, H. Zhang, X. Zhang, Q. Du, Z. Liang, Elimination pathways of systemically delivered siRNA. *Mol. Ther.* **19**, 381–385 (2011).
18. J. E. Green, M. A. Shibata, K. Yoshidome, M. L. Liu, C. Jorcyk, M. R. Anver, J. Wigginton, R. Wiltrout, E. Shibata, S. Kaczmarczyk, W. Wang, Z. Y. Liu, A. Calvo, C. Couldrey, The C3(1)/SV40 T-antigen transgenic mouse model of mammary cancer: Ductal epithelial cell targeting with multistage progression to carcinoma. *Oncogene* **19**, 1020–1027 (2000).
19. M. A. Shibata, C. L. Jorcyk, M. L. Liu, K. Yoshidome, L. G. Gold, J. E. Green, The C3(1)/SV40 T antigen transgenic mouse model of prostate and mammary cancer. *Toxicol. Pathol.* **26**, 177–182 (1998).
20. D. di Bernardo, M. J. Thompson, T. S. Gardner, S. E. Chobot, E. L. Eastwood, A. P. Wojtovich, S. J. Elliott, S. E. Schaus, J. J. Collins, Chemogenomic profiling on a genome-wide scale using reverse-engineered gene networks. *Nat. Biotechnol.* **23**, 377–383 (2005).
21. H. Xing, T. S. Gardner, The mode-of-action by network identification (MNI) algorithm: A network biology approach for molecular target identification. *Nat. Protoc.* **1**, 2551–2554 (2006).
22. M. Cantile, G. Pettinato, A. Procino, I. Feliciello, L. Cindolo, C. Cillo, In vivo expression of the whole HOX gene network in human breast cancer. *Eur. J. Cancer* **39**, 257–264 (2003).
23. A. Chariot, V. Castronovo, Detection of HOXA1 expression in human breast cancer. *Biochem. Biophys. Res. Commun.* **222**, 292–297 (1996).
24. X. Zhang, T. Zhu, Y. Chen, H. C. Mertani, K. O. Lee, P. E. Lobie, Human growth hormone-regulated HOXA1 is a human mammary epithelial oncogene. *J. Biol. Chem.* **278**, 7580–7590 (2003).
25. X. J. Ma, Z. Wang, P. D. Ryan, S. J. Isakoff, A. Barmettler, A. Fuller, B. Muir, G. Mohapatra, R. Salunga, J. T. Tuggle, Y. Tran, D. Tran, A. Tassin, P. Amon, W. Wang, W. Wang, E. Enright, K. Stecker, E. Estepa-Sabal, B. Smith, J. Younger, U. Balis, J. Michaelson, A. Bhan, K. Habin, T. M. Baer, J. Brugge, D. A. Haber, M. G. Erlander, D. C. Sgroi, A two-gene expression ratio predicts clinical outcome in breast cancer patients treated with tamoxifen. *Cancer Cell* **5**, 607–616 (2004).
26. C. M. Perou, T. Sørlie, M. B. Eisen, M. van de Rijn, S. S. Jeffrey, C. A. Rees, J. R. Pollack, D. T. Ross, H. Johnsen, L. A. Akslen, O. Fluge, A. Pergamenschikov, C. Williams, S. X. Zhu, P. E. Lønning, A. L. Børresen-Dale, P. O. Brown, D. Botstein, Molecular portraits of human breast tumours. *Nature* **406**, 747–752 (2000).
27. J. R. Pollack, T. Sørlie, C. M. Perou, C. A. Rees, S. S. Jeffrey, P. E. Lonning, R. Tibshirani, D. Botstein, A. L. Børresen-Dale, P. O. Brown, Microarray analysis reveals a major direct role of DNA copy number alteration in the transcriptional program of human breast tumors. *Proc. Natl. Acad. Sci. U.S.A.* **99**, 12963–12968 (2002).
28. L. Radvanyi, D. Singh-Sandhu, S. Gallichan, C. Lovitt, A. Pedyczak, G. Mallo, K. Gish, K. Kwok, W. Hanna, J. Zubovits, J. Armes, D. Venter, J. Hakimi, J. Shortreed, M. Donovan, M. Parrington, P. Dunn, R. Oomen, J. Tartaglia, N. L. Berinstein, The gene associated with trichorhinophalangeal syndrome in humans is overexpressed in breast cancer. *Proc. Natl. Acad. Sci. U.S.A.* **102**, 11005–11010 (2005).
29. S. Ramaswamy, K. N. Ross, E. S. Lander, T. R. Golub, A molecular signature of metastasis in primary solid tumors. *Nat. Genet.* **33**, 49–54 (2003).
30. T. Sørlie, C. M. Perou, R. Tibshirani, T. Aas, S. Geisler, H. Johnsen, T. Hastie, M. B. Eisen, M. van de Rijn, S. S. Jeffrey, T. Thorsen, H. Quist, J. C. Matese, P. O. Brown, D. Botstein, P. E. Lønning, A. L. Børresen-Dale, Gene expression patterns of breast carcinomas distinguish tumor subclasses with clinical implications. *Proc. Natl. Acad. Sci. U.S.A.* **98**, 10869–10874 (2001).
31. Y. H. Huang, Y. Bao, W. Peng, M. Goldberg, K. Love, D. A. Bumcrot, G. Cole, R. Langer, D. G. Anderson, J. A. Sawicki, Claudin-3 gene silencing with siRNA suppresses ovarian tumor growth and metastasis. *Proc. Natl. Acad. Sci. U.S.A.* **106**, 3426–3430 (2009).
32. K. M. Mohankumar, X. Q. Xu, T. Zhu, N. Kannan, L. D. Miller, E. T. Liu, P. D. Gluckman, S. Sukumar, B. S. Emerald, P. E. Lobie, HOXA1-stimulated oncogenicity is mediated by selective upregulation of components of the p44/42 MAP kinase pathway in human mammary carcinoma cells. *Oncogene* **26**, 3998–4008 (2007).
33. J. R. Barrow, H. S. Stadler, M. R. Capecchi, Roles of *Hoxa1* and *Hoxa2* in patterning the early hindbrain of the mouse. *Development* **127**, 933–944 (2000).
34. N. Shah, S. Sukumar, The Hox genes and their roles in oncogenesis. *Nat. Rev. Cancer* **10**, 361–371 (2010).
35. T. Svingen, K. F. Tonissen, Altered HOX gene expression in human skin and breast cancer cells. *Cancer Biol. Ther.* **2**, 518–523 (2003).
36. M. Abe, J. Hamada, O. Takahashi, Y. Takahashi, M. Tada, M. Miyamoto, T. Morikawa, S. Kondo, T. Moriuchi, Disordered expression of HOX genes in human non-small cell lung cancer. *Oncol. Rep.* **15**, 797–802 (2006).
37. J. L. Chen, J. Li, K. J. Kiriluk, A. M. Rosen, G. P. Paner, T. Antic, Y. A. Lussier, D. J. Vander Griend, Deregulation of a Hox protein regulatory network spanning prostate cancer initiation and progression. *Clin. Cancer Res.* **18**, 4291–4302 (2012).
38. K. L. Rice, J. D. Licht, *HOX* deregulation in acute myeloid leukemia. *J. Clin. Invest.* **117**, 865–868 (2007).
39. Y. Friedmann, C. A. Daniel, P. Strickland, C. W. Daniel, *Hox* genes in normal and neoplastic mouse mammary gland. *Cancer Res.* **54**, 5981–5985 (1994).
40. M. T. Lewis, Homeobox genes in mammary gland development and neoplasia. *Breast Cancer Res.* **2**, 158–169 (2000).
41. M. Flanagan, S. Love, E. S. Hwang, Status of intraductal therapy for ductal carcinoma in situ. *Curr. Breast Cancer Rep.* **2**, 75–82 (2010).
42. S. M. Love, W. Zhang, E. J. Gordon, J. Rao, H. Yang, J. Li, B. Zhang, X. Wang, G. Chen, B. Zhang, A feasibility study of the intraductal administration of chemotherapy. *Cancer Prev. Res.* **6**, 51–58 (2013).
43. V. Stearns, T. Mori, L. K. Jacobs, N. F. Khouri, E. Gabrielson, T. Yoshida, S. L. Kominsky, D. L. Huso, S. Jeter, P. Powers, K. Tarpinian, R. J. Brown, J. R. Lange, M. A. Rudek, Z. Zhang, T. N. Tsangaris, S. Sukumar, Preclinical and clinical evaluation of intraductally administered agents in early breast cancer. *Sci. Transl. Med.* **3**, 106ra108 (2011).
44. S. Murata, S. L. Kominsky, M. Vali, Z. Zhang, E. Garrett-Mayer, D. Korz, D. Huso, S. D. Baker, J. Barber, E. Jaffee, R. T. Reilly, S. Sukumar, Ductal access for prevention and therapy of mammary tumors. *Cancer Res.* **66**, 638–645 (2006).
45. Y. S. Chun, T. Yoshida, T. Mori, D. L. Huso, Z. Zhang, V. Stearns, B. Perkins, R. J. Jones, S. Sukumar, Intraductally administered pegylated liposomal doxorubicin reduces mammary stem cell function in the mammary gland but in the long term, induces malignant tumors. *Breast Cancer Res. Treat.* **135**, 201–208 (2012).

46. R. G. Holzer, C. MacDougall, G. Cortright, K. Atwood, J. E. Green, C. L. Jorcyk, Development and characterization of a progressive series of mammary adenocarcinoma cell lines derived from the C3(1)/SV40 large T-antigen transgenic mouse model. *Breast Cancer Res. Treat.* **77**, 65–76 (2003).
47. A. Akinc, A. Zumbuehl, M. Goldberg, E. S. Leshchiner, V. Busini, N. Hossain, S. A. Bacallado, D. N. Nguyen, J. Fuller, R. Alvarez, A. Borodovsky, T. Borland, R. Constien, A. de Fougerolles, J. R. Dorkin, K. Narayanannair Jayaprakash, M. Jayaraman, M. John, V. Koteliansky, M. Manoharan, L. Nechev, J. Qin, T. Racie, D. Raitcheva, K. G. Rajeev, D. W. Sah, J. Soutschek, I. Toudjarska, H. P. Vornlocher, T. S. Zimmermann, R. Langer, D. G. Anderson, A combinatorial library of lipid-like materials for delivery of RNAi therapeutics. *Nat. Biotechnol.* **26**, 561–569 (2008).
48. S. Krause, A. Brock, D. Ingber, Intraductal injection for localized drug delivery to the mouse mammary gland. *J. Vis. Exp.* **80**, e50692 (2013).

Acknowledgments: We thank C. Jorcyk (Boise State University) for M6 and M6C cells, K. Freeman for Eph4 cells, and H. Tobin and H. Lurvey for excellent technical assistance. **Funding:** This study was funded by the Department of Defense Breast Cancer Innovator Award W81XWH-08-1-0659 (to D.E.I.) and the Wyss Institute for Biologically Inspired Engineering at Harvard University. J.J.C. and H.L. were supported by the Howard Hughes Medical Institute, SysCODE (Systems-based Consortium for Organ Design & Engineering), and NIH grant RL1DE019021. The postdoctoral training of S.K. was supported by the Susan G. Komen Foundation (KG101329). H.L. is supported by the Mayo Clinic Center for Individualized Medicine. Microarray analysis was performed at the Mental Retardation and Developmental Disabilities Research Center Molecular Genetics Core Facility at Children's Hospital Boston (NIH-P30-HD18655) and has been deposited with the NCBI GEO (http://www.ncbi.nlm.nih.gov/geo/) under accession number GSE50813. **Author contributions:** A.B. designed and performed the experiments, and drafted the manuscript with input from the other authors; S.K. performed animal studies; H.L. performed the computational analyses; M.S.G. prepared siRNA lipidoid nanoparticles; M.K. performed immunohistochemical staining; and D.E.I. and J.J.C. conceived the study and led the manuscript preparation effort. **Competing interests:** The authors declare that they have no competing financial interests. **Data and materials availability:** No data require purchase. Materials transfer agreement is required for transfer of materials.

Submitted 16 July 2013
Accepted 5 November 2013
Published 1 January 2014
10.1126/scitranslmed.3007048

Citation: A. Brock, S. Krause, H. Li, M. Kowalski, M. S. Goldberg, J. J. Collins, D. E. Ingber, Silencing *HoxA1* by intraductal injection of siRNA lipidoid nanoparticles prevents mammary tumor progression in mice. *Sci. Transl. Med.* **6**, 217ra2 (2014).